Simulated Phase Evolution Rewinding (SPHERE): A Technique for Reducing B_0 Inhomogeneity Effects in MR Images

Yasser M. Kadah, Xiaoping Hu

A novel method for reducing field inhomogeneity effects in magnetic resonance images is described in this paper. Observing that image degradation arises from B_0 inhomogeneity-induced phase accrual during data acquisition, the present method numerically rewinds the accumulated phase in the *k*-space data based on an initial estimate of the image and a corresponding field map. The rewinding process generates a corrected *k*-space data set that is subsequently Fourier transformed to produce the final image. In this paper, a theoretical analysis of the method and applications of the technique to magnetic resonance imaging data are presented. The theoretical analysis of the method indicates that it is a general approach applicable to a variety of sequences. Results obtained by applying the method to experimental data acquired with single-shot echo-planar imaging, segmented echo-planar imaging with centric reordering, and spiral sequences demonstrate that it is robust in reducing image degradation induced by B_0 inhomogeneity.

Key words: EPI; spiral; image distortion; image processing; B_0 inhomogeneity.

INTRODUCTION

In magnetic resonance imaging, linear magnetic field gradients are applied to achieve spatial encoding. Such an encoding scheme can be sensitive to static field (B_0) inhomogeneity because the B_0 inhomogeneity effects cannot be distinguished from that of the applied gradients. Consequently, image degradation often arises from B_0 inhomogeneity. In spin-echo or single-shot echo-planar imaging (EPI) sequences, in which the traversal of the k space in a given direction is monotonic and linearly related to the time within the sampling window, image degradation appears as spatial distortions. For example, in a single-shot EPI sequence, image distortions can appear in both the readout direction and the phase-encoding direction but are more prominent along the phase-encoding direction because the k-space traversal along phase-encoding takes a relatively longer time. As a result of the distortion, local displacement and intensity modulation are present in the image. Intuitively, the spatial displacement is a result of the local off-resonance frequency, whereas the intensity modulation reflects the derivative of the static field. For applications such as stereotactic localization, geometric accuracy is essential, and B_0 inhomogeneity-induced distortions can be unacceptable (1, 2). In functional MRI, severe distortions in EPI images make anatomic referencing using images obtained with other sequences difficult. Therefore, in many applications of MRI, it is desirable to correct for such distortions. Many authors have suggested and implemented methods for correcting B_0 inhomogeneity-induced spatial shift. In most of these methods, a field map is first derived and utilized in the correction. The field map is either used in the spatial domain to estimate the pixel shifts and unwarp the image accordingly (3–6), or used to modify the k-space data during image reconstruction as in the conjugate phase method (7). The pixel shifting can be equivalently accomplished by a linear phase-modulation through the Fourier shift theorem (8). Others have proposed to use images obtained with alternative gradient polarity and derive the corrected image based on a matching procedure between these images (9, 10).

For more complicated sequences, such as centrally reordered segmented EPI (11), gradient- and spin-echo (GRASE) (12, 13), and spiral, where the relationship between the k-space variable and the time within the acquisition window is not linear or monotonic, the B_0 inhomogeneity effect generally leads to a position-dependent local blurring. Such blurring degrades the spatial resolution achievable with these sequences and needs to be reduced to ensure proper spatial resolution. Several methods have been previously described to address the B_0 inhomogeneity problem in spiral sequences (14–16).

In this work, a general approach for reducing B_0 inhomogeneity effects is described. Observing that in MRI, image degradation due to B_0 inhomogeneity arises from the phase accrual in the long data acquisition window, the present approach introduces the concept of phase rewinding by numerically generating a corrected k-space data set based on an initial estimate of the image and a corresponding field map. After phase rewinding, the k-space data set is Fourier transformed to obtain the corrected image. This approach is termed simulated phase evolution rewinding (SPHERE). In the simplest case, SPHERE resembles the Fourier space shift technique introduced by Weisskoff and Davis (8). However, because SPHERE is conceptualized based on the data acquisition process, it is more general and can be applied to other data acquisition schemes. With proper approximations, the computational complexity is comparable to existing techniques (14–16). This paper describes the technical details of SPHERE and provides a rigorous and complete

MRM 38:615–627 (1997)

From the Biomedical Engineering Program, Department of Radiology, and Center for Magnetic Resonance Research, University of Minnesota Medical School, Minneapolis, Minnesota.

Address correspondence to: Xiaoping Hu, Ph.D., Center for Magnetic Resonance Research, 385 East River Road, Minneapolis, MN 55455.

Received October 9, 1996; revised January 20; 1997; accepted March 20, 1997.

This work was supported by National Institutes of Health grants RR08079 and MH55346 (X.H.) and the IDB Merit Scholarship Program (Y.K.).

0740-3194/97 $3.00

theoretical analysis of the technique. The technique is demonstrated by applying it to correct data obtained with single-shot EPI, centric reordered segmented EPI, and spiral sequences.

THEORY

Consider imaging an object $f(\mathbf{r})$ in the presence of magnetic field inhomogeneity $\Delta B(\mathbf{r})$, which corresponds to an off-resonance frequency $\Delta\nu(\mathbf{r}) = \gamma\Delta B(\mathbf{r})$. Ignoring relaxation effects, gradient imperfections, and T_2^* decay, the signal acquired from this object in the presence of Fourier encoding takes the form:

$$D(\mathbf{k}) = \int f(\mathbf{r}) e^{2\pi j \Delta\nu(\mathbf{r}) t(\mathbf{k}) - 2\pi j \mathbf{k}\cdot\mathbf{r}} d\mathbf{r} \qquad [1]$$

where $D(\mathbf{k})$ is the signal sampled with Fourier encoding $\mathbf{k}$, and $t(\mathbf{k})$ is the time at which $D(\mathbf{k})$ is sampled. When the data acquisition window is small relative to the off-resonance frequency, i.e., $(\max(t(\mathbf{k})) - \min(t(\mathbf{k}))) \cdot |\Delta\nu(\mathbf{r})| \ll 1$, the inhomogeneity term in Eq. [1] is essentially independent of $\mathbf{k}$ and leads to a TE-dependent phase factor in the estimate of $f(\mathbf{r})$ that is eliminated in the magnitude image. For sequences such as EPI and spiral in which the data acquisition window is very wide (e.g., 100 ms) and the inhomogeneity term is $\mathbf{k}$ dependent, severe image distortion and blurring can occur.

To remove the inhomogeneity-induced effects in the acquired data, it is necessary to undo the phase effect in Eq. [1], which depends on both $\mathbf{r}$ and $\mathbf{k}$. An exact solution to this problem can be achieved only if $f(\mathbf{r})$ and $\Delta\nu(\mathbf{r})$ are known. In this work, an approximate solution is derived based on this principle. Without the exact knowledge of $f(\mathbf{r})$, an initial estimate from the acquired data, $\hat{f}(\mathbf{r})$, is used. An estimate of the off-resonance function, $\Delta\hat{f}(\mathbf{r})$, is derived from the phase-difference of images acquired at two different echo times using the sequence under consideration. With this approach, $\Delta\hat{\nu}(\mathbf{r})$ is affected by the B_0 inhomogeneity but exactly registered with the initial estimate of $\hat{f}(\mathbf{r})$. Mathematically, the rewinding process can be described as

$$\hat{D}(\mathbf{k}) = \int \hat{f}(\mathbf{r}) e^{-2\pi j \Delta\hat{\nu}(\mathbf{r}) t(\mathbf{k}) - 2\pi j \mathbf{k}\cdot\mathbf{r}} d\mathbf{r} \qquad [2]$$

The rewinding process generates a simulated k-space data set, $\hat{D}(\mathbf{k})$, which is subsequently used to reconstruct the final image. An intuitive interpretation of the correction technique is that it essentially redistributes $\hat{f}(\mathbf{r})$ according to the off-resonance frequency map and the characteristics of the imaging process. A block diagram of the correction process is shown in Fig. 1.

The effect of the phase-rewinding process described in Eq. [2] can be understood with the following analysis in which a 1D object is considered without loss of generality. The initial estimate, $\hat{f}(x)$, can be expressed as:

$$\hat{f}(x) = \int_{-\infty}^{\infty} e^{+j2\pi kx} \int_{-\infty}^{\infty} f(\alpha) \cdot e^{j2\pi\Delta\hat{\nu}(\alpha)t(k)} e^{-j2\pi k\alpha}\, d\alpha\, dk \qquad [3]$$

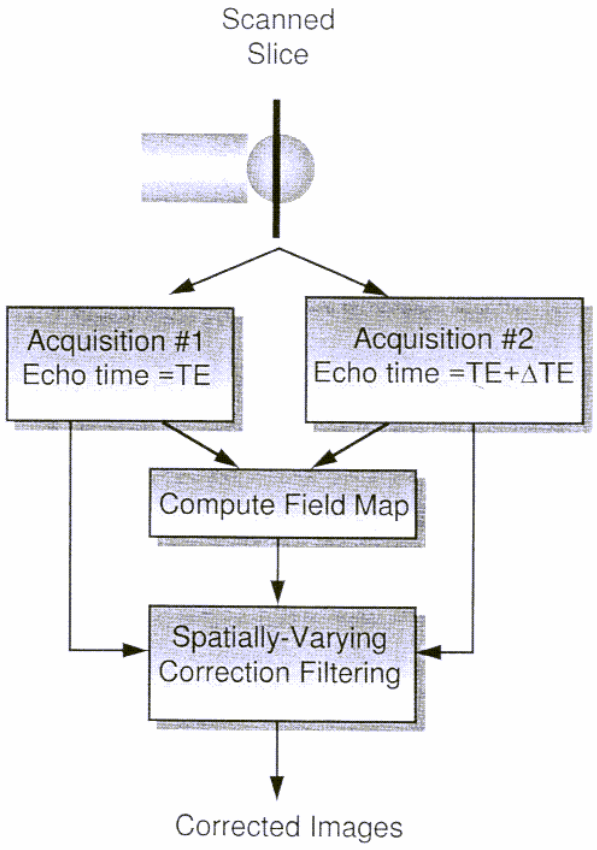

FIG. 1. A block diagram of SPHERE.

which can be expressed as the inner product of $f(x)$ and a *distortion kernel* such that,

$$\hat{f}(x) = \int_{-\infty}^{\infty} f(\alpha) \cdot \Psi(\alpha, x) d\alpha = \langle f, \Psi \rangle \qquad [4]$$

with

$$\Psi(\alpha, x) = \int_{-\infty}^{\infty} e^{j2\pi\Delta\hat{\nu}(\alpha)t(k)} \cdot e^{-j2\pi k(\alpha - x)} dk \qquad [5]$$

being the distortion kernel. Note that Eq. [4] is not a simple convolution because $\Psi(\alpha, x)$ is not shift invariant. If the inhomogeneity function is zero, the distortion kernel is a δ-function (the identity kernel). Otherwise, it is sparse in general and could be ill conditioned. It is straightforward to show that the correction method described above applies a *correction kernel*,

$$\Gamma(\alpha, x) = \int_{-\infty}^{\infty} e^{-j2\pi\Delta\hat{\nu}(\alpha)t(k)} \cdot e^{-j2\pi k(\alpha - x)} dk \qquad [6]$$

to $\hat{f}(x)$ such that

$$\hat{f}_c(x) = \int_{-\infty}^{\infty} \Gamma(\alpha, x) \cdot \hat{f}(\alpha) d\alpha \qquad [7]$$

Combining Eqs. [4] and [7], we have

$$\hat{f}_c(x) = \int_{-\infty}^{\infty} f(\xi) \cdot \Phi(\xi, x) d\xi \qquad [8]$$

where

$$\Phi(\xi, x) = \langle \Gamma, \Psi \rangle = \int_{-\infty}^{\infty} \Gamma(\alpha, x) \cdot \Psi(\xi, \alpha)\, d\alpha \qquad [9]$$

Eqs. [7] and [8] indicate that the effect of SPHERE is to process $\hat{f}(x)$ with a restoration kernel such that the resultant estimate, $\hat{f}_c(x)$, corresponds to the original function integrated with a compound kernel, Φ.

The effectiveness of the correction process (in terms of the residual error) is fully described by the compound kernel. For complete restoration, the compound kernel should be the identity kernel. Before a theoretical analysis is provided, the above formalism is illustrated with an example. In this example, discrete versions of the three kernels described above were computed for a practical case. A one-dimensional (1D) line along the phase-encoding direction is considered for a segmented EPI sequence with centric reordering. The distortion kernel is calculated using the field map derived from FLASH images obtained at two echo times (Fig. 2a), and the correction kernel is calculated based on the field map derived from two segmented EPI images at different echo times (Fig. 2b). The overall compound kernel is the result of the matrix product of the two. The result of the calculation is illustrated in Fig. 2c. In this representation an identity kernel should be a diagonal line, and any deviation from the diagonal indicates a deviation from the identity kernel. In particular, the splitting in the distortion kernel (Fig. 2a) shows the dispersion effect of the large field inhomogeneity in that region. In the correction kernel (Fig. 2b), a similar splitting in the same region compensates that in the distortion kernel. Consequently, the compound kernel (Fig. 2c) is very close to the identity kernel except at a small region where the inhomogeneity effect is very severe and significantly violates the working conditions for the technique described below. This practical example demonstrates the ability of SPHERE to reduce the inhomogeneity distortions under realistic conditions. The formal description of the performance of SPHERE and these conditions are presented in the following section.

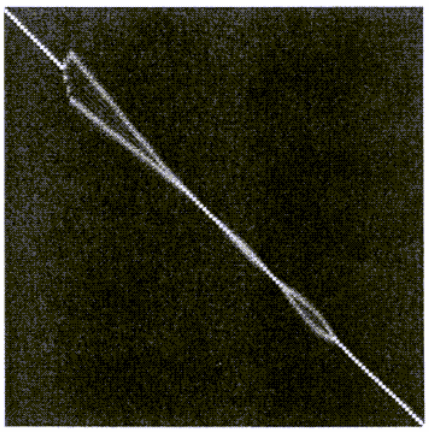

a

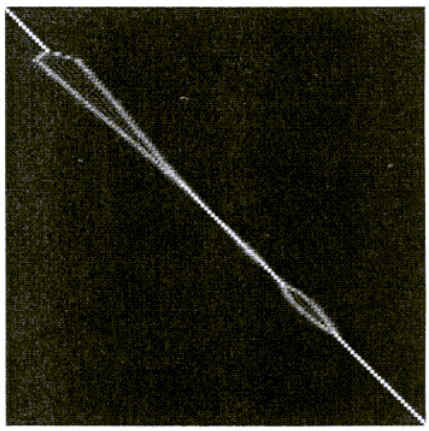

b

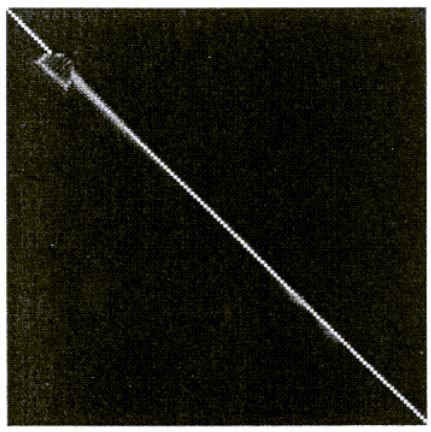

c

FIG. 2. An illustration of the kernels encountered with the proposed SPHERE formalism in segmented EPI where (a) is the distortion kernel, (b) is the correction kernel used with SPHERE, and (c) is the resultant compound kernel, which indicates a good correction.

PERFORMANCE ANALYSIS OF SPHERE

In the following, a theoretical analysis of SPHERE is presented. Because the compound kernel is determined by $t(\mathbf{k})$, which is sequence dependent, two special cases will be considered first to illustrate the idea before the general case is considered. The first special case concerns the single-shot EPI in which only the phase-encoding direction needs to be considered. In this case, $t(k)$ is a linear function of k, i.e., $t(k) = ak$, where a is a constant. Despite its simplicity, this case is presented to illustrate the principle of the subsequent analysis. The distortion and correction kernels take the following forms:

$$\Psi(\alpha, x) = \delta(x - \alpha - a\Delta\nu(\alpha))$$

$$\text{and } \Gamma(\alpha, x) = \delta(x - \alpha + a\Delta\hat{\nu}(\alpha)) \qquad [10]$$

It follows that the compound kernel is:

$$\Phi(\alpha, x) = \delta(x - \alpha - a\Delta\nu(\alpha) + a\Delta\hat{\nu}(\alpha + a\Delta\nu(\alpha))) \quad [11]$$

When the distortion is in the form of a simple shift or when signals arising from different regions in the original image do not overlap, the terms containing the off-resonance effect in Eq. [11] cancel, and the compound kernel becomes the identity kernel, leading to complete restoration. In practice, this condition may be violated in certain areas such as tissue area boundaries. Only a partial correction can be achieved in these locations.

The second case concerns a segmented EPI sequences with centric reordering (see Fig. 1 of ref. 11 for k-space coverage). This case is more complex because the overlap of the distortion shifts from neighboring pixels cannot be avoided in general. The 1D formalism is still valid here because the field inhomogeneity mainly affects the phase-encoding direction. The form of $t(k)$ in this case is a linear function of the absolute value of k rather than k itself as in the first case. The inhomogeneity phase function can be expressed as the sum of two linear terms over two nonoverlapping windows of the k space. That is,

$$e^{j2\pi\Delta\nu(x)\cdot a|k|} = e^{j2\pi\Delta\nu(x)\cdot ak}\cdot u(k) + e^{-j2\pi\Delta\nu(x)\cdot ak}\cdot u(-k) \quad [12]$$

where $u(k)$ is a unit-step function and a is a constant. The corresponding distortion and correction kernels are:

$$\Psi(\alpha, x) = U_+(x - \alpha - a\Delta\nu(\alpha)) + U_-(x - \alpha + a\Delta\nu(\alpha)) \quad [13]$$

and

$$\Gamma(\alpha, x) = U_+(x - \alpha + a\Delta\hat{\nu}(\alpha)) + U_-(x - \alpha - a\Delta\hat{\nu}(\alpha)) \quad [14]$$

where $U_+(\alpha)$ and $U_-(\alpha)$ are the Fourier transforms of $u(k)$ and $u(-k)$, respectively. It follows from Eqs. [13] and [14] that the compound kernel is a sum of four terms, each corresponding to a possible combination of $U_+(.)$ and $U_-(.)$ in the two kernels. Specifically,

$$\begin{aligned}\Phi(\alpha, x) = &\int_{-\infty}^{\infty} U_+(\beta - \alpha - a\Delta\nu(\alpha))U_+(x - \beta + a\Delta\hat{\nu}(\beta))d\beta \\ &+ \int_{-\infty}^{\infty} U_-(\beta - \alpha + a\Delta\nu(\alpha))U_-(x - \beta - a\Delta\hat{\nu}(\beta))d\beta \\ &+ \int_{-\infty}^{\infty} U_+(\beta - \alpha - a\Delta\nu(\alpha))U_-(x - \beta - a\Delta\hat{\nu}(\beta))d\beta \\ &+ \int_{-\infty}^{\infty} U_-(\beta - \alpha + a\Delta\nu(\alpha))U_+(x - \beta + a\Delta\hat{\nu}(\beta))d\beta\end{aligned} \quad [15]$$

Under the condition that the distortion is nonoverlapping in space (hereafter referred to as the nonoverlapping condition), $\Delta\hat{\nu}(\beta)$ is constant and equal to $\Delta\nu(\alpha)$ within the nonzero portions of the integrands of the compound kernel. Hence, each of these four terms is equivalent to an inner product of shifted versions of $U_+(.)$ and $U_-(.)$. Given that shifted versions of $U_+(.)$ and $U_-(.)$ correspond to $u(k)$ and $u(-k)$ multiplied by linear phase functions in the k space, respectively, the terms containing the multiplication of $U_+(.)$ with $U_-(.)$ vanish because the corresponding k-space functions are orthogonal. For example, the third term in Eq. [15] becomes,

$$\begin{aligned}&\int_{-\infty}^{\infty} U_+(\beta - \alpha - a\Delta\nu(\alpha))U_-(x - \beta - a\Delta\hat{\nu}(\beta))d\beta = \\ &\frac{1}{2\pi}\int_{-\infty}^{\infty} u(k)u(-k)e^{-j2\pi k(-\alpha - 2\pi a\Delta\nu(\alpha))}e^{-j2\pi k(x - 2\pi a\Delta\nu(\alpha))}dk \\ &= 0\end{aligned} \quad [16]$$

This orthogonality can be deduced from the fact that the multiplication of $u(k)$ and $u(-k)$ is zero everywhere regardless of the presence of linear phase multipliers and by invoking Parseval's identity of the Fourier transform (17). The remaining two terms take the form of the autocorrelation of $U_+(\alpha)$ and $U_-(\alpha)$, respectively, resulting in $u(k)$ and $u(-k)$, which add up to a constant in the k-space or a δ-function in the spatial domain. In a mathematical form,

$$\begin{aligned}\Phi(\alpha, x) &= \frac{1}{2\pi}\left(\int_{-\infty}^{\infty} u(k)e^{j2\pi(x-\alpha)k}dk + \int_{-\infty}^{\infty} u(-k)e^{+j2\pi(x-\alpha)k}dk\right) \\ &= \frac{1}{2\pi}\int_{-\infty}^{\infty} e^{j2\pi(x-\alpha)k}dk \\ &= \delta(x - \alpha)\end{aligned} \quad [17]$$

Consequently, the resultant compound kernel under the nonoverlapping condition is an identity kernel, and complete restoration is possible in this case.

In the general case, it can be shown mathematically that SPHERE results in a complete restoration when the resultant spatial distortions are nonoverlapping (see Appendix). This theoretical condition can be approximately satisfied with overlapping distortions when the original function and the field inhomogeneity map are both locally smooth.

In the above analysis, it was shown that the correction kernel was able to restore the true image under the idealized nonoverlapping condition. Without overlapping, the correction kernel was constructed using exact knowledge of the inhomogeneity. In practice, the nonoverlapping condition is usually not fully satisfied. The overlap may introduce some ambiguity in the process of redis-

tributing pixels in the corrected image due to errors in estimating the correction kernel. To see how SPHERE works in practice, the correction process is examined under these nonideal conditions. Specifically, the spatially dependent point spread function (PSF) of the compound kernel is derived and assessed to see how it is affected by practical limitations.

In the following, discrete sampling in the k space is considered, and for simplicity, the field of view is normalized to 1 without loss of generality. To derive the PSF, a single point in the original image located at x_0 is considered. This point is first distorted by the distortion kernel constructed for x_0 and with an inhomogeneity value $\Delta\nu(x_0)$. To calculate the contribution of the original point in the corrected image at any arbitrary point $(x_0 + \Delta x)$, a correction kernel centered at $(x_0 + \Delta x)$ and constructed using an inhomogeneity value of $\Delta\hat{\nu}(x_0 + \Delta x)$ is applied. Expressing $\Delta\nu(x_0 + \Delta x)$ and $\Delta\nu(x_0) + \delta\nu$, the final result can be expressed as a function of both Δx and $\delta\nu$ and defined as the *correction ambiguity function* or CAF(.,.). In a mathematical form,

$$\begin{aligned}\mathrm{CAF}(\Delta x, \delta\nu; x_0) &= \int_{-1/2}^{1/2} \Psi(x_0, \beta) \cdot \Gamma(\beta, x_0 + \Delta x) d\beta \\ &= \int_{-1/2}^{1/2} \Im_{k\to\beta}\{e^{j2\pi\Delta\nu(x_0)t(k)} \cdot e^{-j2\pi k x_0}\}. \\ &\quad \Im_{k\to\beta}\{e^{j2\pi(\Delta\nu(x_0)+\delta\nu)t(k)} \cdot e^{-j2\pi k(x_0+\Delta x)}\}^* \, d\beta\end{aligned} \quad [18]$$

where $\Im_{k\to\beta}\{.\}$ is the inverse Fourier transform from the k domain to the β domain and the forms of $\Psi(\alpha, x)$ and $\Gamma(\alpha, x)$ from Eqs. [5] and [6] are invoked. From Parseval's theorem of the Fourier transform, given two periodic functions $F(x)$ and $G(x)$ and their Fourier transforms as the discrete functions $f(k)$ and $g(k)$, the following identity is true (17):

$$\sum_k f(k) \cdot g^*(k) = \int_{-1/2}^{1/2} F(x) \cdot G^*(x) dx \quad [19]$$

This theorem states that the inner product of two functions does not change when the Fourier transform is applied. Hence, Eq. [18] can be written as:

$$\begin{aligned}\mathrm{CAF}(\Delta x, \delta\nu) &= \sum_k (e^{j2\pi\Delta\nu(x_0)t(k)} e^{-j2\pi k x_0}) \cdot (e^{-j2\pi(\Delta\nu(x_0)+\delta\nu)t(k)} e^{j2\pi k(x_0+\Delta x)}) \\ &= \sum_k e^{-j2\pi\delta\nu \cdot t(k)} \cdot e^{j2\pi k \cdot \Delta x}\end{aligned} \quad [20]$$

Given this form of the ambiguity function, the PSF which is spatially dependent is given by:

$$\mathrm{PSF}(x, x_0, \Delta\hat{\nu}(x) - \Delta\nu(x)) = \mathrm{CAF}(x - x_0, \Delta\hat{\nu}(x) - \Delta\nu(x_0)) \quad [21]$$

With this formalism, the PSF essentially corresponds to a curved profile of the 2D CAF, where the curve is determined by the functional form of $\delta\nu$. Eqs. [20] and [21] allow us to evaluate the PSF for any particular k-space trajectory. When $\delta\nu$, i.e., $(\Delta\hat{\nu}(x) - \Delta\nu(x_0))$, is zero, the ambiguity function approaches a δ function. When $\delta\nu$ is not zero, the ambiguity function is very close to a δ function. In Fig. 3, an example of the correction ambiguity function for the case of a centric-reordered segmented-EPI sequence is presented as a surface plot (Fig. 3a) to depict the relative magnitude of the various components of the function and as a grey scale image (Fig. 3b) to

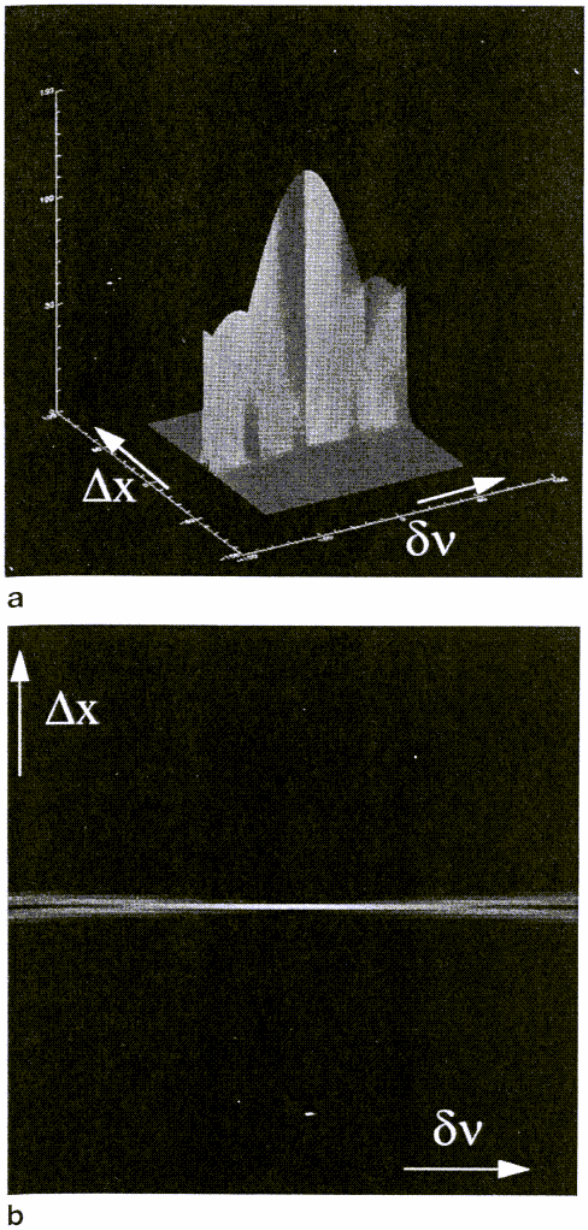

FIG. 3. Illustration of the correction ambiguity function (CAF) for the case of segmented EPI with centric reordering. (a) Surface plot. (b) Image representation.

illustrate the spatial dispersion. The PSF derived for this sequence before and after the correction process are illustrated in Fig. 4a and 4b, respectively. The inhomogeneity was $\Delta\nu = 2/T$ and the correction was applied such that $\delta\nu = 0.5/T$, where T is the data acquisition period. Also, the two-dimensional extension of the above analysis is applied to evaluate the PSF of a spiral sequence with inhomogeneity $\Delta\nu = 2/T$ and after the correction when $\delta\nu = 0.5/T$; the results are shown in Fig. 5. As can be observed, the resultant point spread functions are close to an ideal δ function.

The importance of Eq. [20] lies in that it illustrates when SPHERE is a good approximation. It is a good approximation when $\delta\nu$ $(= \Delta\hat{\nu}(x) - \Delta\nu(x_0))$ is small. Observing that $\Delta\hat{\nu}(x)$ is the result of mixing original signal magnitude, it is therefore bounded by the range of $\Delta\nu(x)$ in a neighborhood defined by the blurring function. Under most practical situations, $\Delta\nu(x)$ is smooth, and $\delta\nu$ is usually small. Therefore, the approximation utilized in SPHERE is valid for most conditions. This observation also explains that the deviation of the compound kernel from the identity kernel in Fig. 2 occurred only in a location where $\delta\nu$ is large.

METHOD

The technique requires an initial estimate of the image and an inhomogeneity map. In this implementation, the inhomogeneity map is derived from the phase difference of two images acquired at different *TE*s with the sequence of interest. The maps are smoothed with a spatial filter to improve the signal-to-noise ratio and thresholded based on the image magnitude to remove the background pixels. To eliminate phase-wrapping in the resultant phase map, Schafer's unwrapping procedure (18) was used. The resultant field map, along with the initial estimate of the image to be corrected, was used in the discrete version of Eq. [2] to generate the simulated *k*-space data for the final image.

Because each point in the *k* space is acquired at a different time in general, the exact implementation of SPHERE calls for a point by point correction, requiring a long reconstruction time. In practice, this stringent requirement can be relaxed to a large extent by suitable approximations based on the characteristics of the sequence of interest. Specifically, to reduce the computational complexity of SPHERE, it is implemented by dividing the data acquisition window into a number of nonoverlapping partitions and treating each partition as an instant, or a time step, in the correction. The computational complexity of SPHERE is thus proportional to the number of time steps rather than the number of *k*-space points. In our implementation of SPHERE for EPI sequences, since the time required to scan individual *k*-space lines along the readout direction is relatively short and the inhomogeneity effects in this direction can be ignored, the *k*-space correction is performed on lines instead of points. In applying SPHERE to spiral scanning, the partitioning is achieved by dividing the *k*-space into equally spaced annular rings where each ring is considered to be acquired instantaneously. Note that this implementation corresponds to a nonuniform partitioning of the data acquisition window that is aimed at emphasizing the correction accuracy in the low *k*-space areas.

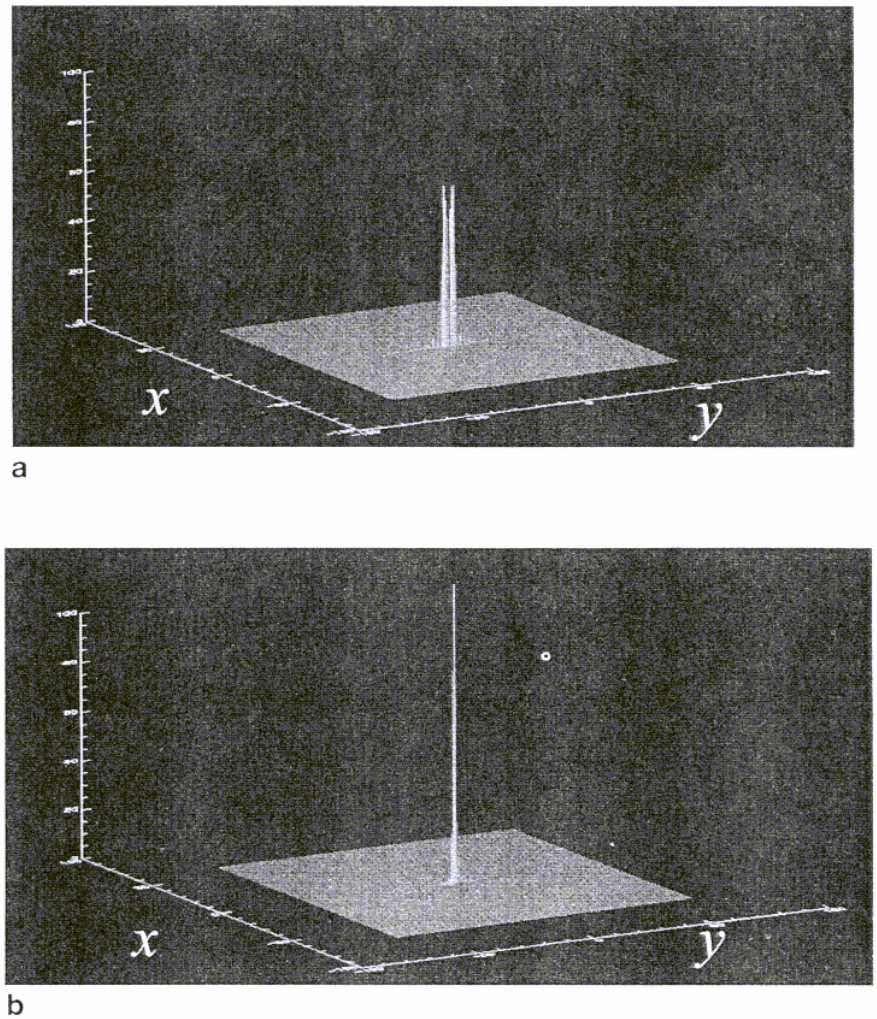

FIG. 4. Illustration of the PSF for the case of segmented EPI with centric reordering. (a) Before correction. (b) After SPHERE correction.

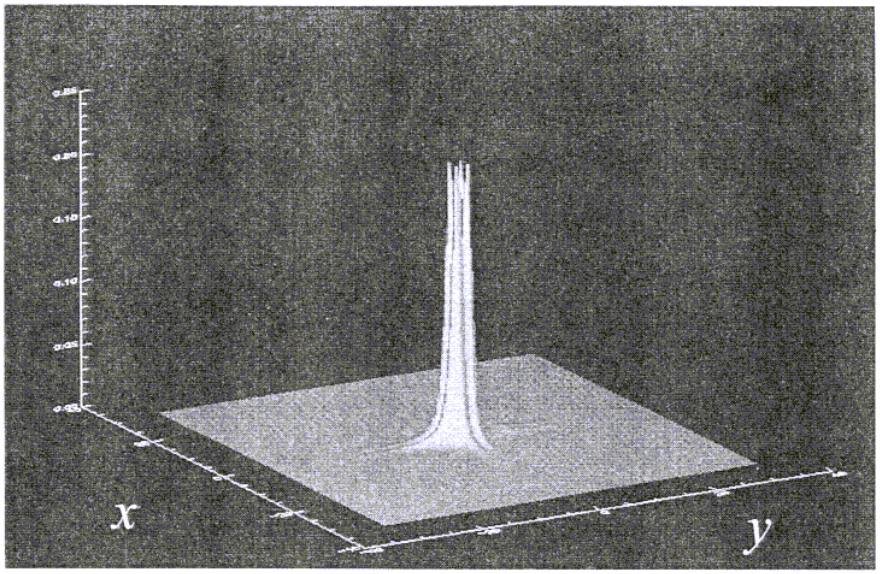

a

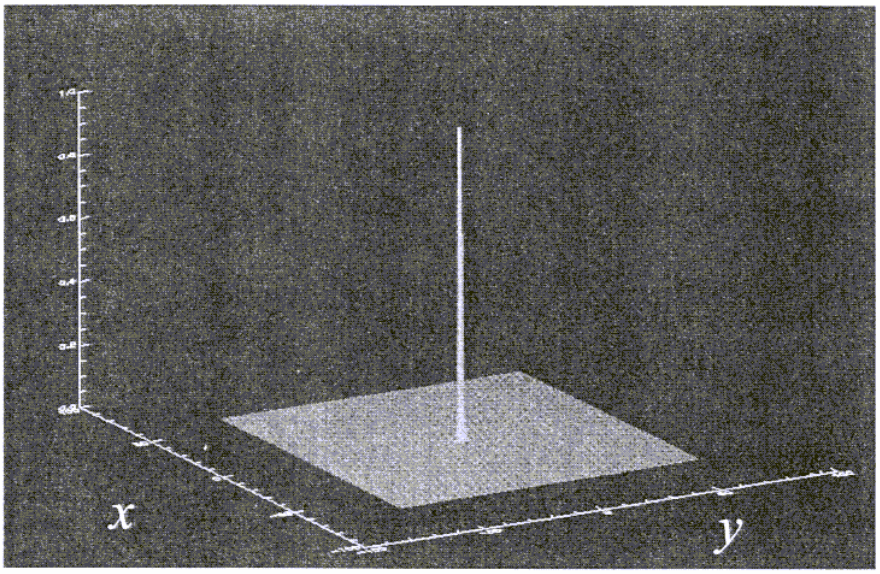

b

FIG. 5. Illustration of the PSF for the case of spiral imaging. (a) Before correction. (b) After SPHERE correction.

To illustrate the performance of this technique, it is applied to data obtained on a 1.5 T Siemens Magnetom Vision MR scanner using sequences in which B_0 inhomogeneity-induced degradation has varying degrees of complexity. The first sequence was a single-shot blipped-EPI sequence. Experimental data were acquired in phantoms and volunteers. For the phantom study, the imaging parameters are *TR*/*TE*, 200/70 ms; blip spacing, 0.96 ms; matrix, 128 × 128; slice thickness, 5 mm; and field of view, 31 × 31 cm. On the volunteers, sagittal and coronal images were obtained with imaging parameters identical to those used in the phantom study.

The second sequence studied was a segmented EPI sequence with centric reordering (11). In this case, the off-resonance degradation is more complicated and leads to a sum of two shifted versions of the original image. Experimental data in both phantoms and normal volunteers were obtained (same imaging parameters as blipped-EPI with two segments). These images were corrected with SPHERE, and the resultant images were compared with images obtained using FLASH.

SPHERE was also applied to image different phantoms as well as normal human volunteers using a spiral imaging sequence. The field map required for correction was obtained from two spiral acquisitions with different echo times. The k space was covered by 16 interleaved spirals, each taking approximately 11 ms. The gradient waveforms used in this sequence were chosen according to previously described spiral scanning methods (19, 20). The imaging parameters were *TR*/*TE*, 1000/6 ms; field of view, 31 × 31 cm; matrix, 128 × 128.

RESULTS

Results obtained from single-shot blipped-EPI studies are presented in Fig. 6. Figure 6d illustrates images obtained using FLASH for comparison. B_0 maps in these slices derived from two single shot EPI images after smoothing and phase unwrapping are shown in Fig. 6a (the shims are somewhat misadjusted in the phantom study to accentuate the off-resonance effect). The B_0 variation was in the range from −126 to +138 Hz for the phantom study and −100 to +100 Hz for the human study. EPI images obtained without correction (Fig. 6b) are highly distorted. Images obtained after line by line correction using SPHERE (128 time steps) (Fig. 6c) are virtually free of geometric distortion and structurally comparable to the corresponding FLASH images (Fig. 6d). Significant improvement can be noted in areas indicated by the arrows. In particular, in the sagittal image obtained from the normal volunteer, substantial distortions in the frontal area of the brain due to the presence

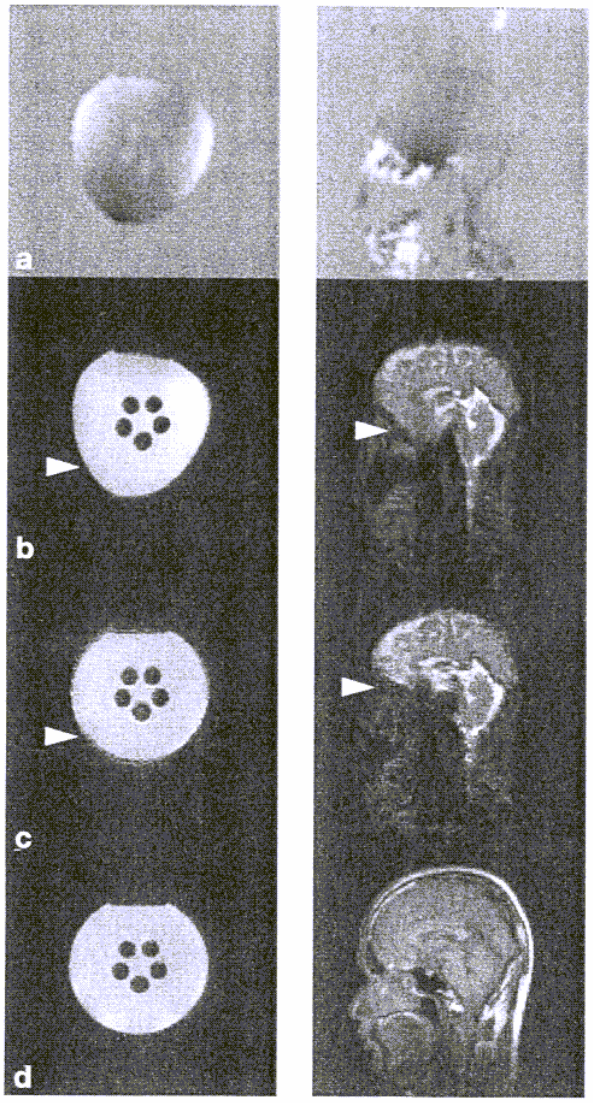

FIG. 6. Phantom and human blipped-EPI data correction results using SPHERE. (a) Computed field maps. (b) Obtained distorted images. (c) Corrected images using SPHERE. (d) Comparison GE images.

of large susceptibility-induced field inhomogeneity were successfully removed in the SPHERE corrected image.

In Fig. 7, results of a phantom study with the centrically reordered segmented EPI sequence are presented. Figure 7b–d illustrate the images obtained with the segmented EPI sequence without correction, with SPHERE correction (64 time steps), and the corresponding FLASH images, respectively. The corresponding field maps are shown in Fig. 7a and the off-resonance frequency varied between −126 to +138 Hz for the first phantom, −33 to +143 Hz for the second, and −164 to +167 Hz for the third. The original images are degraded with spatial distortion as well as blurring. As a result of centric reordering, areas with substantial off-resonance frequency are ghosted on both sides of their original position. The corrected images in panel (c) exhibited both improved geometric accuracy and spatial resolution. In particular, areas that were substantially ghosted are brought back to their original position (see arrows). These images demonstrate that, despite B_0 inhomogeneity-induced blurring, image degradation was significantly reduced by SPHERE. Figure 8 presents results obtained with the same sequence in a normal volunteer. The first two images correspond to sagittal scans obtained with the phase-encoding direction vertical, whereas the third corresponds to a coronal scan with the phase encoding direction horizontal. The field inhomogeneity for the sagittal scans was between −100 and +100 Hz, and that of the coronal scan was between −94 and +100 Hz. Distortions seen in the original images are essentially eliminated, markedly improving the quality of the image. This improvement is particularly evident in the areas marked by the arrows.

The results of a phantom study using a spiral sequence are illustrated in Fig. 9. The B_0 field inhomogeneity maps are shown in Fig. 9a. The off-resonance frequency ranges for the phantoms starting from the leftmost were between −72 to +170 Hz, −89 to +269, and −76 to +247, respectively. The spin-echo comparison images are shown in Fig. 9d. Figure 9b presents the spiral images reconstructed without correction. The images are degraded by blurring arising from the off-resonance effect. The images reconstructed using SPHERE (64 time steps) are shown in Fig. 9c. The blurring in the original images is significantly reduced, providing a better definition of the small structures in the phantoms (see arrows). Figure 10 illustrates the results of applying SPHERE to correct the human brain images obtained with the same spiral sequence. The off-resonance frequency in these slices varied from −228 to +217 Hz, −231 to +213 Hz, and −236 to +200 Hz starting from the leftmost image to the right respectively. The corrected images are sharper than the original images; this improvement in spatial resolution is particularly evident in the locations marked by the arrows.

DISCUSSION

The technique described in this paper for reducing B_0 inhomogeneity degradation in MR images was demonstrated theoretically and experimentally to be effective, even for cases with severe inhomogeneity. The Fourier space shift approach (8), which applies to sequences in which only simple pixel shift occurs, can be shown to be a special case of the present technique. Both SPHERE and the Fourier space shift method avoid the spatial domain interpolation needed by pixel shift-based approaches. The significance of SPHERE is that it not only corrects for B_0 inhomogeneity induced shifts, but also reduces the blurring commonly encountered in complex k-space trajectory sequences. Therefore, the new technique is general and can be applied to all types of sequences.

The correction ambiguity function (CAF) formalism provides a useful way of looking at SPHERE as a space-varying matched filtering process. What the CAF describes is the response of SPHERE to errors in the matched filter estimation and the cross-talk between neighboring matched filters. In the ideal case when there

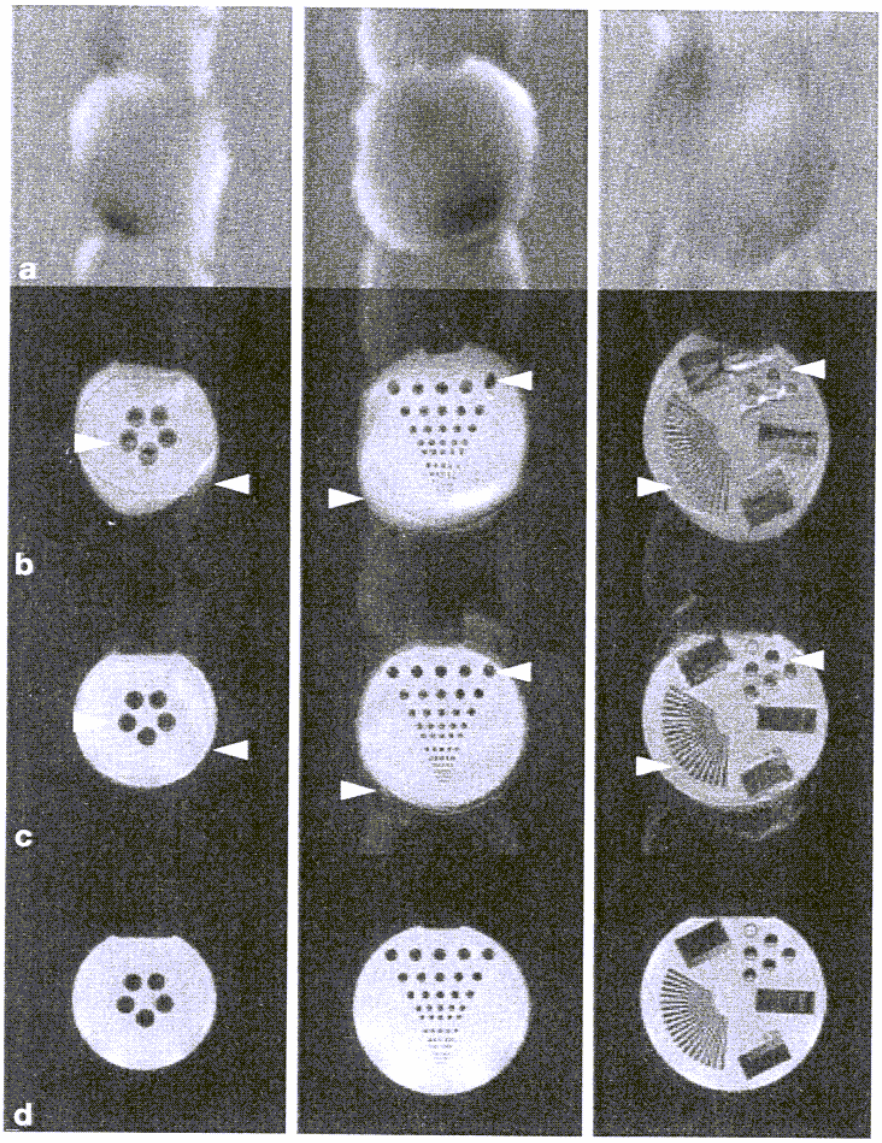

FIG. 7. Results of using SPHERE to correct phantom data acquired with a segmented EPI sequence with centric reordering. (a) Computed field maps. (b) Obtained distorted images. (c) Corrected images using SPHERE. (d) Comparison GE images.

is no overlap for example, the distortion functions to be detected are orthogonal yielding an ideal PSF of a δ function after the correction using SPHERE. On the other hand, when these functions are not orthogonal, there will be a certain amount of cross-talk between neighboring distortions, indicating that an exact correction may not be possible in this case. This point can be readily understood mathematically in the case of overlap by observing that the inverse problem of estimating the corrected image becomes ill posed. This condition can be visualized by looking at the CAF of the imaging system. For example, for segmented EPI with centric reordering shown in Fig. 3, the ideal response is represented by the zero of the δv scale, in which the response is an exact δ function in the Δx direction. When the overlap starts to cause bias errors in the estimation of the correction kernel (or equivalently when δv gets larger), the resultant response begins to deviate from the ideal response, and a finite support function results instead of the ideal δ function. This result is reflected as a weaker response peak magnitude and a wider response bandwidth. When the deviation from the ideal conditions becomes too significant, the correction process may fail to provide good results and a large portion of the original distortion remains as can be seen near the edges of Fig. 3b. Nevertheless, it should be noted that under most practical conditions, the inhomogeneity function is locally smooth, and the correction is expected to be reasonably localized within the middle portion of the CAF, thereby providing effective correction. Even when this condition does not hold, the outcome of the technique can be shown to exhibit a reduced version of the original distortion. Therefore, it is clear that SPHERE is effective in reducing the B_0 inhomogeneity under most practical imaging conditions.

It is interesting to compare SPHERE with other correction techniques in the literature. Many of the available techniques are based on pixel shifting in various forms either in the spatial domain or the frequency domain by using Fourier shift theorem (3–6, 8). These techniques work only with linear k-space trajectory sequences such as blipped-EPI and cannot remove the blur encountered with the more complex imaging sequences such as centric reordered segmented EPI and spiral imaging. On the other hand, the conjugate phase method is based on an approximate inverse transformation from the k-space to the corrected spatial domain and can be used with complex sequences (7). This method requires the acquisition of undistorted field maps, usually obtained using gradient echo sequences, and derives each point in the corrected image from the distorted k-space data and the estimated field inhomogeneity only at that point. In contrast, SPHERE derives each point in the corrected image space in terms of the estimated field inhomogeneity of all points, which is potentially advantageous in addition to being relatively immune to misregistrations between the distorted image and its field map. For example, when the distortion causes pixel shifts into areas

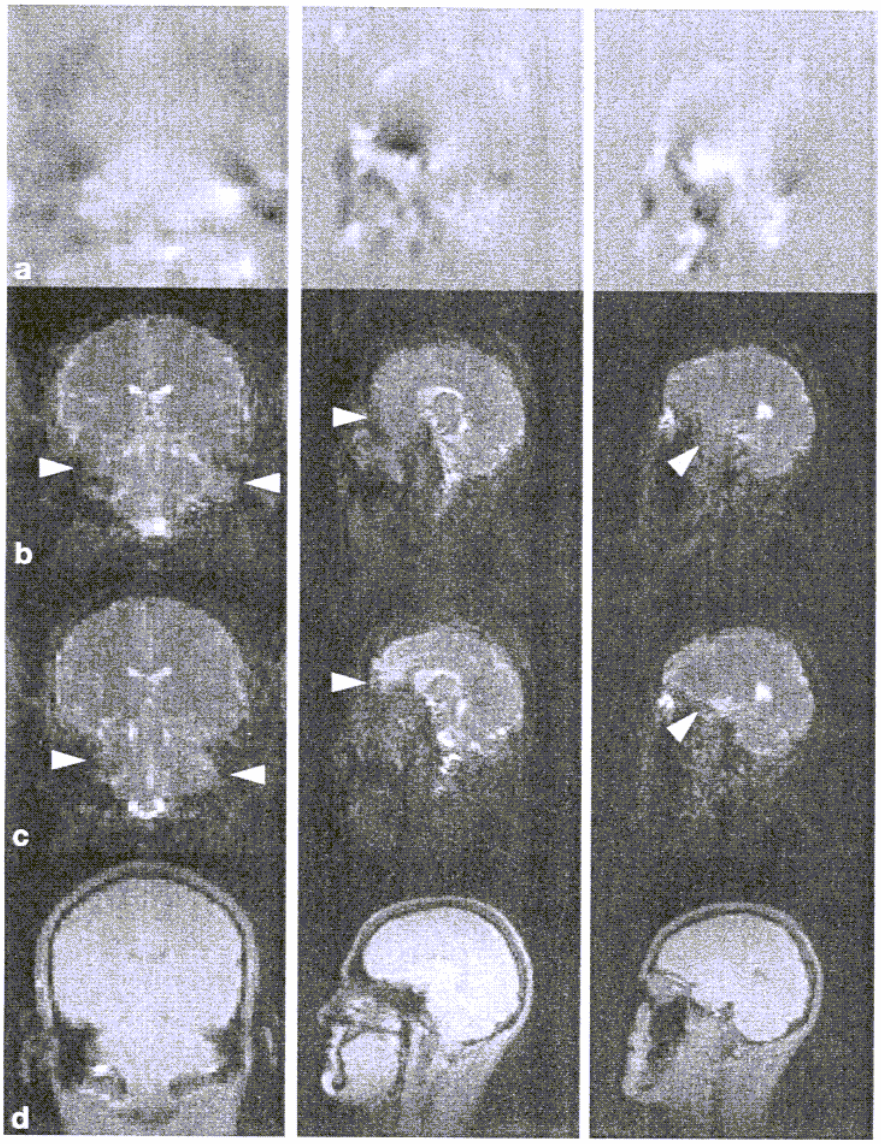

FIG. 8. Results of using SPHERE to correct human brain images acquired with a segmented EPI sequence with centric reordering. (a) Computed field maps. (b) Obtained distorted images. (c) Corrected images using SPHERE. (d) Comparison GE images.

outside the support of the undistorted object, the field map of the undistorted object in this area will be identically zero because these areas will be empty in the gradient echo field mapping images. As a result, the correction procedure in the conjugate phase method will leave these pixels unaltered, which in turn remain as artifacts near the boundaries. In contrast, this problem will not arise in SPHERE because the field map is derived based on the distorted image. An illustration of the comparison of conjugate phase and SPHERE is shown in Fig. 11 in which both methods were applied to the human data of Fig. 8. As can be seen, the edges in the SPHERE-corrected image are better defined when compared with the conjugate phase corrected image (see arrows). This difference between SPHERE and the conjugate phase method also applies to other conjugate phase-based technique such as those currently used for spiral imaging (14, 15). The method in ref. 15 has the advantage of not requiring a field map and therefore, is useful if field mapping is not available. The method described in ref. 16 is quite efficient; however, it is applicable only when the field map is predominantly linear in nature. It should be noted that SPHERE can be readily combined with this method instead of (15) with no additional data acquisition requirements to take advantage of the already available field mapping information.

Two practical scenarios of using SPHERE for dynamic imaging and functional imaging can be envisioned. The first is to acquire a reference scan for the volume of interest using a sequence that has a slightly different echo time from the one used in the actual data acquisition. Each image in the actual data is corrected based on the field map obtained from the image and the corresponding reference scan. Although this scenario requires that the object remains still between the acquisition of the reference data and the subsequent imaging, it has been successfully used with other artifact correction schemes in functional imaging applications (21). The second scenario might be more suitable for dynamic imaging applications in which the imaged object may change dramatically during the acquisition period. In this case, the slice or slices of interest can be scanned with alternative echo times such that all the odd acquisitions correspond to one echo time, whereas the even acquisitions correspond to another slightly different echo time. Any given image with acquisition order n in the obtained sequence of images is corrected based on the field map obtained from the images n and $(n-1)$. This approach allows the correction process to effectively track the changes in the field during the acquisition period because the reference image is also changing with time. Therefore, it is particularly suitable for dynamic imaging applications in which this property provides much more accurate field maps than the fixed reference scan method. It should be noted that these scenarios are also applicable with other correction techniques.

Let us now address the computational complexity of SPHERE. Consider first the 1D case when the distortion

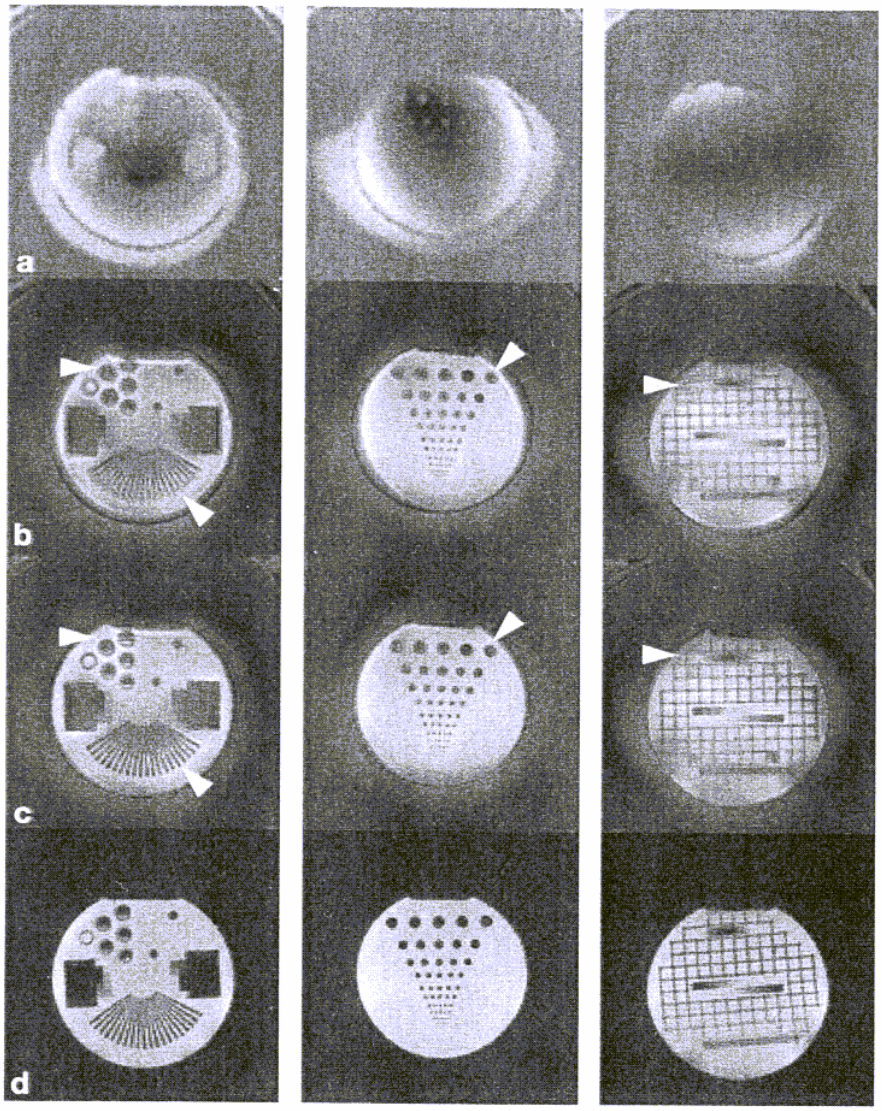

FIG. 9. Results of using SPHERE to correct spiral scans of phantoms. (a) Computed field maps. (b) Obtained distorted images. (c) Corrected images using SPHERE. (d) Comparison SE images.

is negligible along one of the two dimensions of an $M \times N$ image, say the first dimension. The number of time steps used in SPHERE is equal to N. The technique first computes the field map from two images ($O(M \cdot N)$ flops/image). Subsequently, for each line in the k space along the first dimension, a space varying filter is applied to derive the corrected k space ($O(M \cdot N + N \cdot M \cdot \log(M) + M \cdot N \cdot \log(N))$ flops/line, repeated for N lines/image). The corrected image is obtained by applying an inverse Fourier transform to the corrected k space ($O(M \cdot N \cdot \log(N) + N \cdot M \cdot \log(M))$ flops). Hence, the computational complexity for 1D SPHERE is $O(M \cdot N^2 \cdot (\log(M) + \log(N))$ flops/image. Using a similar argument, it can be shown that the complexity for the general case of using L time steps is $O(L \cdot M \cdot N \cdot (\log(M) + \log(N)))$, where L can be chosen by the user according to the desired accuracy/complexity. It should be noted that the step-wise implementation for SPHERE is similar to a method suggested for use with conjugate phase method (14). Such an implementation corresponds to an approximation of 2D SPHERE by repeated applications of 1D SPHERE, providing a compromise between the accuracy and the computational complexity. In such an approximation, the accuracy is determined by the temporal width of each step. Consequently, with segmented data acquisition schemes in which the sampling windows of each segment is reduced by the number of segments, the number of steps in the SPHERE implementation can also be reduced proportionally.

Because the original image is multiplied by simple phase factors in Eq. [2], noise in the original image is not amplified in the final image. However, the presence of noise in the field map will introduce additional noise in the final image. Therefore, in the current implementation, field maps are smoothed and thresholded based on the image magnitude. Several spatial and frequency domain filters were evaluated in this study, and it was found that a smoothing spatial domain kernel with a size of three pixels provided the best results. Our results confirmed that the uncertainties in field maps do not contribute substantially to the noise in the final image. Another effect of noise in the field map arises from changes in the CAF. Any additive noise superimposed on the field map will amount to a shift in the CAF in the direction δv, causing the point spread function to broaden. As a result, additive noise with large variance may bring about some problems in the correction process and must therefore be filtered out. From our experience, the smoothing process described above kept the uncertainty in the field inhomogeneity estimation below 3% introducing negligible blurring in the correction process. Therefore, SPHERE works robustly in the presence of additive noise.

CONCLUSIONS

A novel technique for reducing B_0 inhomogeneity-induced degradation in MR images has been developed. The technique utilizes simulated phase rewinding to

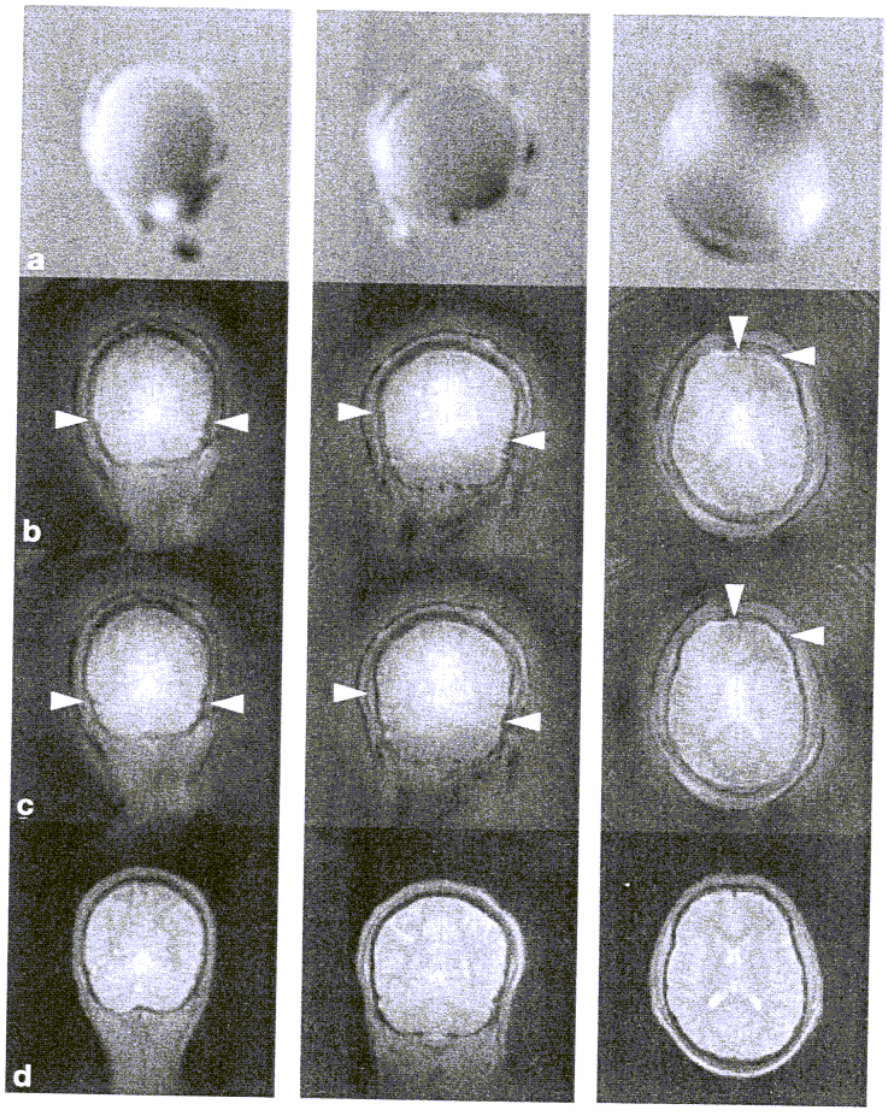

FIG. 10. Results of using SPHERE to correct spiral brain scans of a normal human volunteer. (a) Computed field maps. (b) Obtained distorted images. (c) Corrected images using SPHERE. (d) Comparison GE images.

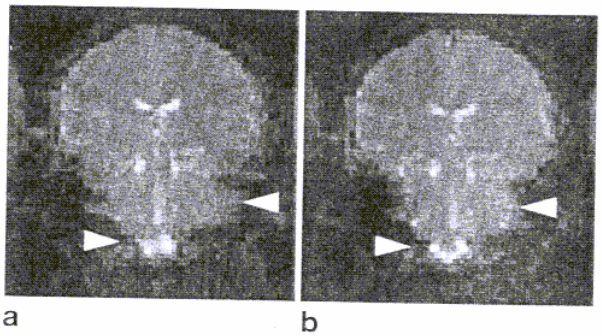

FIG. 11. Comparison of using conjugate phase method (left) and SPHERE correction (right) to correct one of the human brain images in Fig. 9.

generate a corrected k-space data based on the initial estimate of the image and an estimate of the field map. A theoretical analysis of the technique shows that it is exact under ideal conditions of nonoverlapping spatial distortions or constant field inhomogeneity within these distortions. Under practical circumstances, the technique provides a good approximation to the exact correction and its accuracy improves uniformly as the ideal conditions are approached or the field inhomogeneity becomes smoother. The technique was verified on a resolution phantom and successfully applied to head images from normal human subjects. Experimental studies have demonstrated that it is robust for a variety of sequences.

APPENDIX

In the case of an arbitrary k-space trajectory, the complete restoration with SPHERE is first proven when the inhomogeneity phase factor is periodic with period K, which corresponds to the periodic extension with a finite coverage in the k space. Subsequently, the proof is generalized to the infinite coverage by taking the limit as $K \rightarrow \infty$ in the same way the Fourier transform is derived from the Fourier series expansion. When the inhomogeneity factor is periodic, it can be decomposed into a Fourier series. That is,

$$e^{j2\pi\Delta\nu(x)\cdot t(k)} = \sum_n \eta_n(\Delta\nu(x)) \cdot e^{j2\pi ndk} \qquad [A1]$$

and

$$e^{-j2\pi\Delta\hat{\nu}(x)\cdot t(k)} = \sum_n \eta_n^*(\Delta\hat{\nu}(x)) \cdot e^{-j2\pi ndk} \qquad [A2]$$

with fundamental frequency $d = 1/K$. Hence, the corresponding distortion and correction kernels are:

$$\Psi(\alpha, x) = \sum_n \eta_n(\Delta\nu(x)) \cdot \delta(x - \alpha + nd) \qquad [A3]$$

and

$$\Gamma(\alpha, x) = \sum_n \eta_n^*(\Delta\hat{\nu}(x)) \cdot \delta(x - \alpha - nd) \qquad [A4]$$

It follows that:

$$\Phi(\alpha, x) = \sum_m \sum_n \eta_n(\Delta\nu(\alpha - nd))\eta_m^*(\Delta\hat{\nu}(x)) \cdot \delta(x - \alpha + nd - md) \quad [A5]$$

The double sum in Eq. [A5] can be decomposed into two components: the diagonal terms obtained when m = n and the remaining cross-terms. In the ideal case in which there is no overlap which also implies that $\Delta\nu(x - nd) = \Delta\hat{\nu}(x) \forall n \ni \eta_n \neq 0$, the cross-terms vanish based on the following argument. Because both the distortion and correction kernels are linear and bounded (i.e., the result of applying any of them to any function will be finite and can be expressed as a linear combination of elements of that function), operator theory states that the norm of the compound kernel must be less than or equal to the multiplication of their individual norms (22). Given that the norms of the distortion and correction operators are less than or equal to 1 (as can be deduced from the decomposition into orthogonal pure phase kernels and invoking the triangle inequality), the norm of the compound kernel must be less than or equal to one. Now consider the output of applying this kernel. This output is composed of two main components: the zero-shift component corresponding to the diagonal terms of the compound kernel and the nonzero-shift component corresponding to the cross-terms. Because these two components are orthogonal (nonoverlapping in space), the norm of the output will be equal to their geometric sum. It can be shown that the outcome from the diagonal terms alone will have a unity norm. Because the maximum output norm is unity from the definition of the kernel norm and because the norm is always positive, it follows that the norm corresponding to the cross-terms must be zero. As a result, all of its components must be zero from their orthogonality. In other words, the compound kernel is the identity kernel, and complete restoration is achieved.

Now let us consider the generalization of the above solution to the case for which the inhomogeneity phase factor is nonperiodic and has an infinite support. As the period K approaches infinity, the periodic function tends to have only one cycle in the interval $-\infty < k < \infty$ that is identical to inhomogeneity phase factor (23). In approaching the limit, the fundamental frequency d becomes smaller as K is made larger and the frequency spectrum becomes denser. In the limit as $K \to \infty$, the sums in Eqs. [A3–A5] become integrals. Given that the final result of the above analysis is not a function of the fundamental frequency, it can be shown that it is true in the limit as well. That is, complete restoration can be achieved for an arbitrary inhomogeneity phase factor when the nonoverlapping condition is satisfied.

ACKNOWLEDGMENT

The authors thank Dr. Xiasping Ding at Cleveland Clinic for providing the spiral imaging software.

REFERENCES

1. J. Michiels, H. Bosmans, P. Pulgrims, D. Vandermeulen, J. Gybels, G. Marchal, P. Suetens, On the problem of geometric distortion in magnetic resonance images for stereotactic neurosurgery. *Magn. Reson. Imaging* **12**, 749–765 (1994).
2. E. Piovan, P. G. Zampieri, F. Alessandrini, M. A. Gerosa, A. Nicolato, A. Pasoli, R. Foroni, M. G. Giri, A. Bricolo, A. Benati, Quality assessment of magnetic resonance stereotactic localization for gamma knife radiosurgery. *Stereotact. Funct. Neurosurg.* **64**(Suppl. 1), 228–232 (1995).
3. K. Sekihara, M. Kuroda, H. Kohno, Image restoration from non-uniform magnetic field influence for direct Fourier NMR imaging. *Phys. Med. Biol.* **29**, 15–24 (1984).
4. K. Sekihara, S. Matsui, H. Kohno, NMR imaging for magnets with large nonuniformities. *IEEE Trans. Med. Imaging* **MI-4**, 193–199 (1985).
5. K. Sekihara, H. Kohno, Image restoration from nonuniform static field influence in modified echo-planar imaging. *Med. Phys.* **14**, 1087–1089 (1987).
6. P. Jezzard, R. S. Balaban, Correction for geometric distortion in echo planar images from B_0 field variations. *Magn. Reson. Med.* **34**, 65–73 (1995).
7. A. Maeda, K. Sano, T. Yokoyama, Reconstruction by weighted correlation for MRI with time-varying gradients. *IEEE Trans. Med. Imaging* **7**, 26–31 (1988).
8. R. M. Weisskoff, T. L. Davis, Correcting gross distortions on echo planar images. *in* "Proc., SMRM, 11th Annual Meeting, Berlin, 1992," p. 4515.
9. H. Chang, J. M. Fitzpatrick, A technique for accurate magnetic resonance imaging in the presence of field inhomogeneity. *IEEE Trans. Med. Imaging* **11**, 319–329 (1992).
10. R. Bowtell, D. J. O. McIntyre, M. -J. Commandre, P. M. Glover, P. Mansfield, Correction of geometric distortion in echo planar images. *in* "Proc., SMR 2nd Annual Meeting, San Francisco, 1994," p. 411.
11. S. -G. Kim, X. Hu, G. Adriany, K. Ugurbil, Fast interleaved echo-planar imaging with navigator: high resolution anatomic and functional images at 4 Tesla. *Magn. Reson. Med.* **35**, 895–902 (1996).
12. D. A. Feinberg, K. Oshio, GRASE (gradient- and spin-echo) MR imaging: a new fast clinical imaging technique. *Radiology* **181**, 597–602 (1991).
13. J. P. Mugler III, J. R. Brookeman, Off-resonance image artifacts in interleaved-EPI and GRASE pulse sequences. *Magn. Reson. Med.* **36**, 306–313 (1996).
14. D. C. Noll, C. H. Meyer, J. M. Pauly, D. G. Nishimura, A. Macovski, A homogeneity correction method for magnetic resonance imaging with time-varying gradients. *IEEE Trans. Med. Imaging* **10**, 629–637 (1991).
15. D. C. Noll, J. M. Pauly, C. H. Meyer, D. G. Nishimura, A. Macovski, Deblurring for non-2D Fourier transform magnetic resonance imaging. *Magn. Reson. Med.* **25**, 319–333 (1992).
16. P. Irarrazabal, C. H. Meyer, D. G. Nishimura, A. Macovski, Inhomogeneity correction using an estimated linear field map. *Magn. Reson. Med.* **35**, 278–282 (1996).
17. A. V. Oppenheim, R. W. Schafer, *in* "Discrete-Time Signal Processing," Prentice Hall, New Jersey, 1989.
18. J. M. Tribolet, A new phase unwrapping algorithm. *IEEE Trans. Acous. Speech Sign. Proc.* **ASSP-25**, 170–177 (1977).
19. C. J. Hardy, H. E. Cline, Broadband nuclear magnetic resonance pulses with two-dimensional spatial selectivity. *J. Appl. Physiol.* **66**, 1513–1516 (1989).
20. C. H. Meyer, B. S. Hu, D. G. Nishimura, A. Macovski, Fast spiral coronary artery imaging. *Magn. Reson. Med.* **28**, 202–213 (1992).
21. X. Hu, T. H. Le, Artifact reduction in EPI with phase-encoded reference scan. *Magn. Reson. Med.* **36**, 166–171 (1996).
22. B. Choudhary, S. Nanda, *in* "Functional Analysis with Applications," John Wiley & Sons, New York, 1989.
23. B. P. Lathi, *in* "An Introduction to Random Signals and Communications Theory," International Textbook Co., Scranton, PA, 1968.